Identification of Two Electron-Transfer Sites in Ascorbate Peroxidase Using Chemical Modification, Enzyme Kinetics, and Crystallography[†]

David Mandelman, Joumana Jamal, and Thomas L. Poulos*

Department of Molecular Biology and Biochemistry, University of California, Irvine, California 92697-3900

Received August 13, 1998; Revised Manuscript Received October 9, 1998

ABSTRACT: Chemical and mutagenic modification combined with X-ray crystallography has been used to probe the ascorbate binding site in ascorbate peroxidase (APX). Chemical modification of the single Cys residue in APX with Ellman's reagent (DTNB) blocks the ability of APX to oxidize ascorbate but not other small aromatic phenolic substrates. DTNB-modified APX (APX-TNB) exhibits only 1.3% wild-type activity when ascorbate is used as the substrate but full activity when aromatic substrates, guaiacol or pyrogallol, are used. Stopped-flow studies show that APX-TNB reacts normally with peroxide to give compound I but that the rates of reduction of both compounds I and II by ascorbate are dramatically slowed. Conversion of Cys32 to Ser leads to ≈70% drop in ascorbate peroxidase activity with no effect on guaiacol peroxidase activity. These results indicate that uncharged aromatic substrates and the anionic ascorbate molecule interact with different sites on APX. The 2.0 Å X-ray crystal structure of APX-TNB shows clear electron density for the TNB group covalently attached to Cys32 in all four molecules of the asymmetric unit, indicating complete and specific modification. It appears that the ascorbate site is blocked by DTNB modification which is well removed from the exposed δ-heme edge where aromatic substrates are thought to bind. This is the first experimental evidence indicating that ascorbate oxidation does not occur at the exposed heme edge but at an alternate binding site in the vicinity of Cys32 near Arg172 and the heme propionates.

The end product of oxidative phosphorylation (respiration) is the conversion of dioxygen to water with the concomitant production of ATP. A byproduct of this reaction is the superoxide radical which can prove damaging to both proteins and DNA. Cellular mechanisms exist to eliminate these radicals through the intermediate production of H_2O_2 which must be rapidly eliminated. The peroxidase family of hemoproteins are responsible for the rapid reduction of hydrogen peroxide to water at the expense of an electron donor. The general peroxidase mechanism is outlined below:

$$H_2O_2 + Fe^{3+}\ P \rightarrow H_2O + Fe^{4+}{=}O\ P\bullet \text{ (compound I)}$$

$$Fe^{4+}{=}O\ P\bullet + S \rightarrow S\bullet + Fe^{4+}{=}O\ P \text{ (compound II)}$$

$$Fe^{4+}{=}O\ P + S \rightarrow S\bullet + H_2O + Fe^{3+}\ P \text{ (resting state)}$$

The peroxidase reduces hydrogen peroxide to water and in turn is raised 2 oxidizing equiv above its resting state to form compound I (Fe^{4+}═O P•). Two subsequent one-electron reductions return the enzyme back to its initial, ferric, resting state. The first reduction (compound I → II), reduces the radical, P•, back to full valence, P, and the second reduction (compound II → resting) reduces the oxyferryl center, Fe^{4+}═O, back to a ferric heme, Fe^{3+}, with the concomitant protonation and release of the oxygen atom as H_2O.

Many peroxidases lack specificity with respect to reducing substrates. In general, the cellular or extracellular location determines the peroxidase redox partner. For instance, plant ascorbate peroxidase (APX)[1] uses ascorbate to eliminate hydrogen peroxide because of the relatively high levels of ascorbate (50 mM in chloroplasts) in plant cells (*1*). Nevertheless, APX also can oxidize traditional aromatic peroxidase substrates such as guaiacol and pyrogallol at rates comparable to those observed when ascorbate is the substrate (*2*). Since ascorbate is an anion and the aromatic substrates are neutral, the question arises as to whether these substrates interact with the same sites on APX.

Determining where substrates bind and transfer electrons is a longstanding problem in peroxidase research. Since the elucidation of the cytochrome *c* peroxidase (CCP) crystal structure in 1980 (*3*), modeling (*4*) and X-ray crystallography (*5*) have been used to try and reveal the binding interactions between a peroxidase and its redox partner. Unfortunately, CCP is unusual in that it uses another protein as a redox partner rather than small aromatic substrates. In this respect, horseradish peroxidase (HRP) represents a larger cross section of peroxidases that oxidize small molecules. In HRP, suicide substrate inhibition resulting in the addition of organic groups to the δ-meso carbon of the heme results in loss of

[†] This work was supported by National Institutes of Health Grant GM42614. D.M. was partially supported by National Institutes of Health Training Grant GM07311-22.

* To whom correspondence should be addressed at the Department of Molecular Biology and Biochemistry, University of California, Irvine, CA 92697-3900. Fax: (949) 824-3280. Email: poulos@uci.edu.

[1] Abbreviations: APX, ascorbate peroxidase; DTNB (Ellman's reagent), 5,5′-dithiobis(2-nitrobenzoic acid); APX-TNB, APX chemically modified with DTNB; CCP, cytochrome *c* peroxidase; HRP, horseradish peroxidase; BHA, benzhydroxamic acid.

10.1021/bi981958y CCC: $15.00
Published on Web 11/25/1998

activity by sterically blocking access of the substrate to the heme edge (*6*). In addition, the crystal structure of HRP complexed with the inhibitor benzhydroxamic acid (BHA) (*7*) shows binding near the exposed heme edge.

Ascorbate peroxidase is generally considered to be similar to HRP in its interactions with substrates. Modeling combined with NMR and spectral methods have implicated the exposed δ-meso edge of the heme in APX as the site of ascorbate binding (*8*). Thus, both HRP and APX appear to bind substrates at the same site. However, in CCP, reconstitution with heme prosthetic groups chemically modified at the γ and δ edges has provided evidence for multiple electron-transfer sites in this peroxidase (*9*). In this example, guaiacol activity was adversely affected by δ-meso-heme edge modification, and cytochrome *c* activity was blocked by γ-meso-heme edge modification.

One of the characteristic differences between the ascorbate and guaiacol peroxidases is the differential sensitivity toward thiol modification. APX from different sources has been shown to undergo varying degrees of inactivation by such reagents as *p*-chloromercuribenzoate (pCMB) and DTNB whereas the activity of guaiacol peroxidases remains unaffected by thiol derivatization (*10*). Although Asada et al. (*11*) attributed the loss in activity to the possible participation of Cys in the formation of compound I, we considered the possibility that the single Cys32 in APX might be part of specific ascorbate binding site. Here we report kinetic and crystallographic analyses of APX selectively modified at Cys32 by chemical and mutagenic means to test the possible roles of Cys32 in APX catalysis.

MATERIALS AND METHODS

Materials. MilliPore filtered water was used in the preparation of all buffers and reagents. Potassium phosphate, trizma base, poly(ethylene glycol) (PEG) 3350, H_2O_2 (30%), guaiacol, pyrogallol, DTNB, and sodium ascorbate were purchased from Sigma. Potassium ferrocyanide was purchased from Fisher. Mutagenic oligos were purchased from Operon Technologies.

Mutagenesis and Expression. The Cys32Ser mutagenesis was performed using overlapping PCR (*12*). In the first round of PCR, one reaction consisted of the oligos (5′pmal) 5′-GG-GTCAACCATCCAAACCGTTCG-3′ and (AS Cys32Ser) 5′-GAGGAGCGCTTTTCTTCTC-3′; the other reaction had the oligos (3′pmal) 5′-GGGGTCAGGTGGGACCACCGCGC-3′ and (Cys32Ser-sense) 5′-GAGAAGAAAAGCGCTCCTC-3′. PCR consisted of 25 cycles of 94 °C, 1 min; 60 °C, 1 min; 72 °C, 2.5 min. The reactions were run on 1% agarose gels, and the PCR products were excised, Genecleaned (Bio101), and used as templates for the second round of PCR using the 5′pmal and 3′pmal oligos. After the second round of PCR, the product was cloned into the pMal-C2 expression vector at the *Xba*I and *Sac*I sites. Mutations were verified by dideoxy sequencing (*13*) using the Sequenase kit (V. 2.0, United States Biochemicals).

APX and Cys32Ser were expressed and purified as previously described (*14*) using the pMal fusion protein system (New England Biolabs). Protein concentration was determined using an extinction coefficient of 9.1×10^4 M^{-1} cm^{-1} at 403 nm. Proteins were flash-frozen in liquid N_2 and stored at −70 °C in 50 mM KPO_4, pH 7.0.

Preparation of TNB-Modified APX. Wild-type APX was diluted to a final concentration of 325 μM in 200 mM Tris, pH 8.5. DTNB in the same buffer was added to a final concentration of 12.5 mM, and the reaction was allowed to incubate at room temperature for 45 min. It was previously confirmed that modification went to completion in less time with a lower DTNB concentration (data not shown). Free DTNB and TNB were removed by desalting the reaction over a 5 mL Pharmacia desalting column attached to an FPLC (Pharmacia) flowing at 2 mL/min. The column was equilibrated in 50 mM KPO_4, pH 7.0.

Steady-State Kinetics. Stocks of pyrogallol, sodium ascorbate, potassium ferrocyanide, H_2O_2, and enzyme dilutions were prepared in a buffer of 50 mM KPO_4, pH 7.0, 0.1 mM EDTA. Guaiacol stock was prepared in buffer with 30% ethanol. Assays were performed at 23 °C on a Cary 3 UV−Vis spectrophotometer (Varian Inc.) controlled by PC under the Cary Windows 95 kinetics software package, version 1.0. The 1 mL reactions were initiated in the quartz cuvette by the addition of 90 μM H_2O_2, and oxidation was monitored by the change in absorbance. The wavelengths and extinction coefficients used for the various substrates were as follows: ascorbate, $\epsilon_{290} = 2.8$ mM^{-1} cm^{-1}; guaiacol, $\epsilon_{470} = 26.6$ mM^{-1} cm^{-1}; potassium ferrocyanide, $\epsilon_{420} = 1$ mM^{-1} cm^{-1}; pyrogallol, $\epsilon_{430} = 2.47$ mM^{-1} cm^{-1}. Activity was determined by dividing the ΔAbs by ϵ. k_{cat} was calculated by dividing the units of activity by the millimolar concentration of enzyme used in the assay. All values are the mean of three independent assays, and error bars represent the standard deviation.

Transient-State Kinetics. Stopped-flow spectroscopy was performed in a Hi-Tech SF-51/SU-40 with the sample syringes maintained at 20 °C via a circulating water bath. APX was diluted to 2 μM in 50 mM KPO_4, pH 7.0, 0.1 mM EDTA and loaded into syringe 1. For compound I formation, H_2O_2 was loaded into syringe 2, and the samples were rapidly mixed by the application of 40 psi of N_2 gas pressure to both syringes simultaneously. The final concentration of the reactants was half the original concentration. Absorbance changes were monitored at 411 nm and relayed to a PC computer running Hi-Tech stopped-flow software for DOS, version 1.0. The data were fit to first-order reaction equations of the type: $y = \Delta Y \exp(k_{obs}x + b)$, where k_{obs} is the pseudo-first-order rate constant. For compound I reduction, syringe 2 contained 25 μM H_2O_2 and ascorbate, and absorbance was monitored at 424 nm. For compound II reduction, syringe 2 contained ascorbate, and absorbance was monitored at 421 nm. In addition, syringe 1 contained a mixture of 2 μM APX + 4 μM H_2O_2 that was allowed to age for 2 min to allow complete conversion to compound II prior to analysis. Prior spectral analysis had shown that APX compound II is a stable intermediate for up to 1 h. In general, the analyses were complete in under 20 min following compound II formation.

Cryocrystallography. Crystals of Cys32Ser and APX-TNB were grown as previously described (*14*) with one round of touch-seeding and, if necessary, one round of macro-seeding to obtain diffraction quality crystals. Prior to diffraction experiments, crystals were soaked for 2−4 h at room temperature in mother liquor plus 20% ethylene glycol to serve as a cryoprotectant against freezing-induced cracking of the crystals. Data were collected on a Rigaku R-Axis IV imaging plate system equipped with liquid N_2 cryogenics to

Table 1: Summary of Data Collection Statistics and Crystallographic Refinement

	Cys32Ser[a]	APX-TNB[a]
a (Å)	130.8	130.9
b (Å)	52.1	51.9
c (Å)	168.1	168.4
β (deg)	107.5	107.3
reflections observed	295309	211012
unique reflections	84330	69115
*R*sym[b]	7.4	8.5
% overall completeness	85.1	93.6
% complete (highest resolution shell)	59.2 (1.94−1.90)	84 (2.03−2.00)
R-factor[c]	20.1	20.1
% reflections with $I/\sigma I \geq 2$	97.3	78.0
reflections used for refinement, $\|F\| > 2\sigma\|F\|$	84325	69115
RMS[d] deviations, bonds (Å)	0.007	0.008
RMS[d] deviations, angles (deg)	1.31	1.34

[a] Cryogenic conditions as described under Materials and Methods. [b] $R_{sym} = \sum|I_i - \langle I_i \rangle|/\sum I_i$, where I_i is the intensity of the *i*th observation and $\langle I_i \rangle$ is the mean intensity. [c] $R = \sum||F_o| - |F_c||/\sum|F_o|$. [d] The RMS deviations of bond parameters represent the root-mean-square deviations from ideal values.

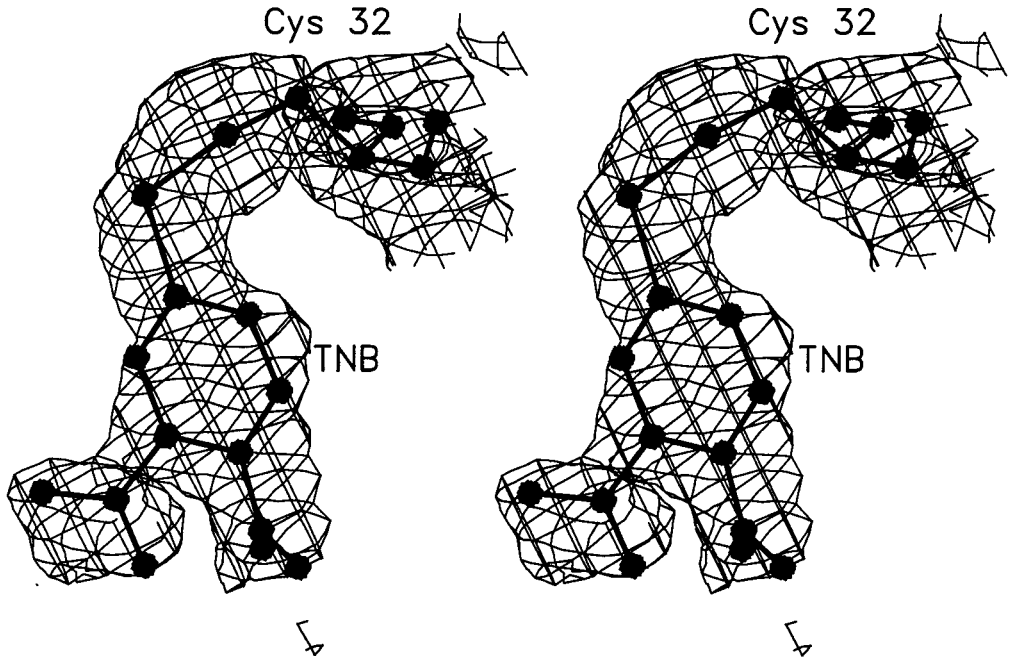

FIGURE 1: Stereo figure of the Cys32-TNB omit electron density map contoured at 1σ. All figures were prepared with either Molscript (*25*) or Setor (*26*).

maintain the crystal frozen during data collection. The detector was placed at 15 cm, and 180° of data was collected at 0.5° oscillations for APX-TNB. For Cys32Ser, data were collected at 0.25° oscillations. A complete data set was collected with one crystal, data were integrated and reduced with Denzo (Z. Otwinowski), and the reflection intensities were scaled using Scalepack (Z. Otwinowski). Both sets of crystals were monoclinic with the same unit cell and belonged to space group *C2*. The reflection file was converted to XPLOR format using CCP4 (*15*). Difference Fourier maps and data refinement were performed in XPLOR (*16*). Molecular modeling was carried out in TOM/FRODO 3.0 (*17*). The TNB molecule was constructed and energy-minimized in Insight II (Ver. 2.3.0, Biosym Technologies, 1993).

RESULTS

The Crystal Structure of APX-TNB and Cys32Ser. APX-TNB crystallized under the same conditions as the wild-type protein, and the data indexed identically in the same space group, *C2*. The data were refined from 10 to 2.0 Å and initially modeled after the wild-type structure, and difference maps were used to properly position the TNB molecule into its electron density. The final *R*-factor for the refined structure with the modeled TNB adduct was 20.1% (Table 1). Figure 1 is an omit electron density map in the vicinity of Cys32. The only appreciable difference density is in the vicinity of Cys32 with continuous electron density between the Cys32 side chain and TNB indicating that the S−S bond has formed. The disulfide bond between TNB and Cys32 was modeled after the average bond length of ≈2.05 Å and bond angles seen in most disulfide-containing proteins. In order for the S−S bond to form, the χ1 angle of Cys32 must twist ≈180° from its partially buried orientation in the wild-type structure. As shown in Figure 2, the TNB carboxyl group is within H-bonding distance of the guanidinium group of Arg172. Overall, the structure shows complete and specific modifica-

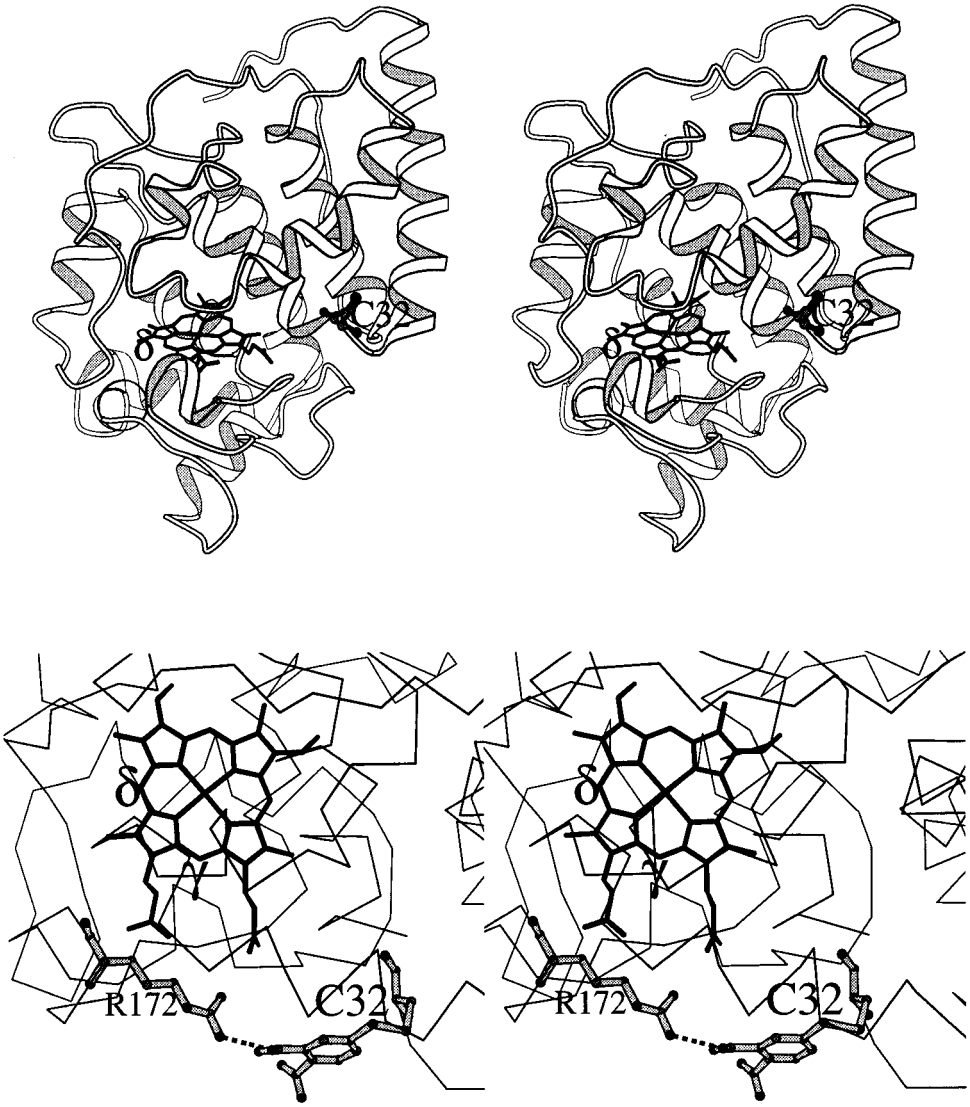

FIGURE 2: The top diagram is a stereoview of the native APX structure showing the location of Cys32 and the δ-heme edge which is the favored site of interaction for small organic substrates. The bottom diagram is a stereoview of the TNB-modified APX viewed along the distal heme surface. The interaction between the TNB carboxylate and Arg172 is highlighted by the dashed line. The δ- and γ-heme edges are labeled.

tion of Cys32 with no other changes in regions outside of the immediate vicinity of Cys32.

For the Cys32Ser mutant, the only significant change was negative electron density corresponding to a decrease in the number of electrons when sulfur is replaced by an oxygen atom. As shown in Figure 3, Cys32 points in to a hydrophobic patch formed by Phe26, Ile27, and Ile36. Replacement of Cys32 with Ser should weaken these interactions although this is not reflected in any significant difference between the wild-type and mutant structures. The final *R*-factor for the Cys32Ser structure was 20.1% (Table 1).

Spectral Properties. Figure 4 shows the UV−Vis absorbance spectra of wild-type APX, Cys32Ser, and APX-TNB. The solid lines indicate the resting-state spectra and show that neither mutagenesis nor chemical modification of Cys32 shifts the Soret peak away from the wild-type value of 403 nm. The R_z value of heme proteins is used to assess purity and extent of heme reconstitution and is a ratio of absorbances at 403 and 280 nm. All three proteins had a R_z of 2.1−2.2, indicating the proteins were fully reconstituted and pure. APX-TNB has a slightly red-shifted Soret peak by approximately 3 nm with a slight deformation of the peak shoulder between 350 and 400 nm. This is due to the absorbance properties of the TNB adduct in the visible region and not to perturbation of the heme absorbance properties.

The dotted lines in Figure 4 are the spectra taken 1 min after the addition of a molar equivalent of H_2O_2. In all three cases, the Soret peak shifts by 10 nm to 413 nm, the peak width decreases, and the peak rises. In addition, the appearance of the α/β bands at 532 and 560 nm is indicative of native APX compound II formation. Compound I in APX is a short-lived porphyrin-based radical (*18*) whose spectrum most likely resembles that of HRP (unpublished data). Its spectrum decays too rapidly to capture by conventional spectroscopic means, and therefore the more stable compound II spectrum is used as a qualitative reference of the reactivity of APX with H_2O_2. Stopped-flow techniques, though, can be used to assess the rate of compound I formation.

Rate of Compound I Formation. The transient-state kinetics of compound I formation were measured by stopped-flow spectroscopy. Figure 5 shows the dependence of the first-

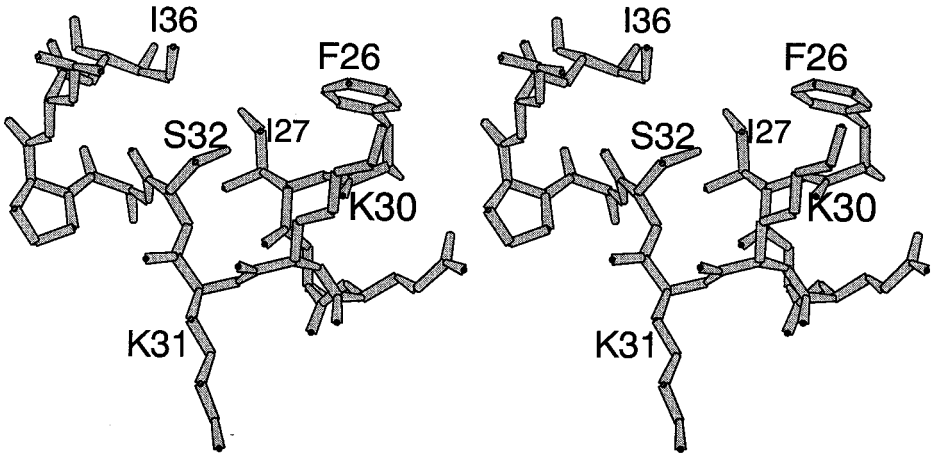

FIGURE 3: Stereoview of the wild-type structure in the vicinity of Cys32. The Cys32Ser mutant structure is not shown since the two structures superimpose with no changes in the vicinity of the mutation or elsewhere in the structure.

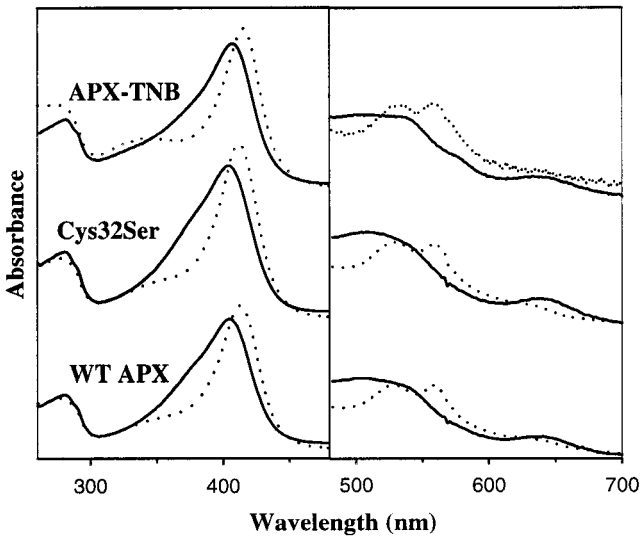

FIGURE 4: UV−Vis spectra of wild-type APX, Cys32Ser, and APX-TNB. The resting-state enzyme (solid lines) was diluted in 50 mM KPO_4, pH 7.0, and compound II (dotted lines) was formed after the addition of 1.1 molar equiv of H_2O_2 and waiting 1 min before taking the spectra.

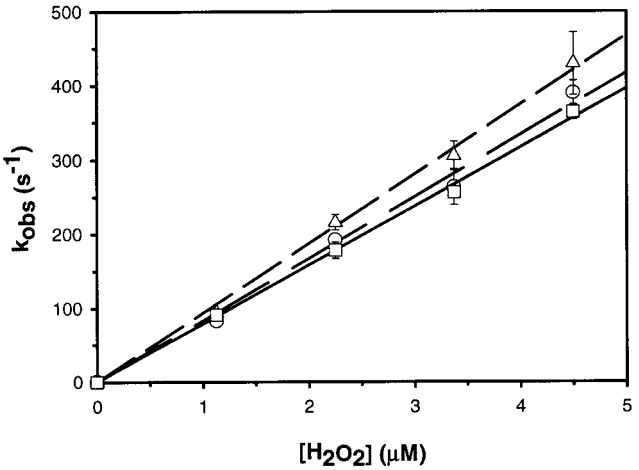

FIGURE 5: Transient-state kinetics of compound I formation in wild-type APX (○), Cys32Ser (△), and APX-TNB (□). Compound I formation was monitored at 411 nm, 20 °C.

order rate constant, k_{obs}, on peroxide concentration. All three proteins exhibited nearly identical second-order rate constants of compound I formation (Table 2): 8.3×10^7, 9.4×10^7, and 7.9×10^7 M^{-1} s^{-1} for wild type, Cys32Ser, and APX-TNB, respectively.

Ascorbate Peroxidase Activity. Figure 6 shows the steady-state kinetics of ascorbate oxidation by APX, Cys32Ser, and APX-TNB. The wild-type rates obtained in the assay were identical to those previously published (*19*) and display non-Michaelis−Menten kinetics. The wild-type and Cys32Ser curves did show saturation, but only the initial linear portions of the curves were compared. The effect of DTNB modification on APX reduced the activity to 1.3% that of wild-type activity, and the Cys32Ser mutant had one-third wild-type activity (Table 2).

To determine what step or steps in the catalytic cycle were affected by DTNB modification, stopped-flow experiments were carried out to determine the rate of compounds I and II reduction by ascorbate. In Figure 7 are shown the data for the conversion of compound I to compound II. Linear regression fits to the data yielded second-order rate constants of 3.4×10^7, 1.7×10^7, and 1.6×10^6 M^{-1} s^{-1} for wild type, Cys32Ser, and APX-TNB, respectively. Thus, Cys32Ser and APX-TNB have 50% and 5%, respectively, the activity of wild-type APX (Table 2). The second-order rate of 1.6×10^6 M^{-1} s^{-1} for APX-TNB is still too rapid to account for the attenuated activity seen in the steady-state data, indicating that the conversion of compound I to II is not rate-limiting under steady-state conditions.

The relatively slow rate of conversion of compound II back to resting-state enzyme seen in Figure 8 indicates this is the rate-limiting step in the catalytic mechanism and correlates well with what is seen in the steady-state data. Both wild type and the Cys32Ser mutant exhibit saturation kinetics with increasing ascorbate concentration, but the relatively slow conversion of APX-TNB II back to resting, even at 20-fold higher ascorbate concentration, does not approach saturation. While the reduction of compound II to resting state is not a second-order reaction and the saturation behavior indicates formation of a substrate−compound II complex, the slopes of the linear regions of the plots in Figure 8 were used as a basis for comparison. Analysis of these slopes yields values of 6.0×10^4, 3.5×10^4, and 8.3×10^2 M^{-1} s^{-1} for wild type, Cys32Ser, and APX-TNB, respectively (Table 2). Again, TNB modification of APX reduces activity to 1.4% that of wild type.

Table 2: Steady-State and Transient-State Rates of Oxidation by Wild-Type and Modified APX

	wild type	Cys32Ser	APX-TNB
	Steady-State		
ascorbate[a] ($\times 10^3$ M^{-1} s^{-1})	1900	580	2.5
guaiacol[c] (s^{-1})	52.9	103.9	80.3
	Transient-State (Ascorbate)		
compound I formation[b] ($\times 10^7$ M^{-1} s^{-1})	8.3	9.4	7.9
compound I reduction[b] ($\times 10^6$ M^{-1} s^{-1})	34	17	1.6
compound II reduction[a] ($\times 10^2$ M^{-1} s^{-1})	600	350	8.3

[a] Analysis done on the linear portion of a saturating curve. [b] Linear second-order reaction. [c] Fit with Michaelis−Menten equation.

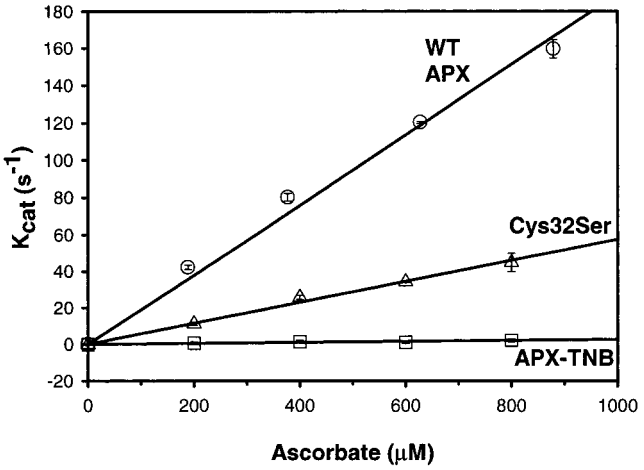

FIGURE 6: Ascorbate oxidation rates by wild-type APX, Cys32Ser, and APX-TNB. Wild-type APX (○) was assayed at a concentration of 26 nM, Cys32Ser (△) was assayed at a concentration of 29.6 nM, and APX-TNB (□) was assayed at a concentration of 24.6 nM.

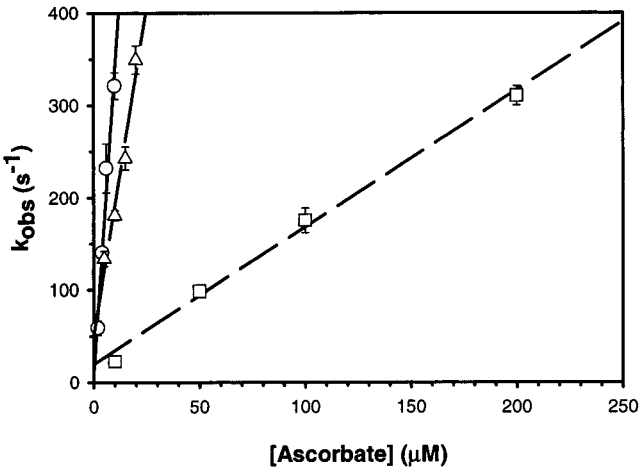

FIGURE 7: Transient-state kinetics of compound I reduction in wild-type APX (○), Cys32Ser (△), and APX-TNB (□). Compound I reduction was monitored at 424 nm, 20 °C.

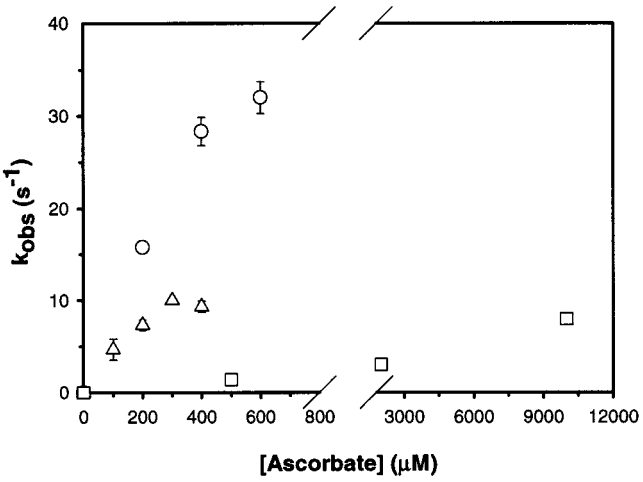

FIGURE 8: Transient-state kinetics of compound II reduction in wild-type APX (○), Cys32Ser (△), and APX-TNB (□). Compound II reduction was monitored at 421 nm, 20 °C.

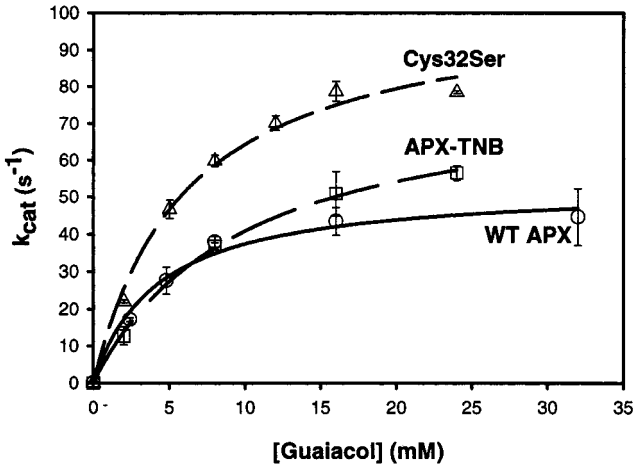

FIGURE 9: Guaiacol oxidation rates by wild-type APX, Cys32Ser, and APX-TNB. Wild-type APX (○) was assayed at a concentration of 26 nM, Cys32Ser (△) was assayed at a concentration of 11.1 nM, and APX-TNB (□) was assayed at a concentration of 24.6 nM.

If ascorbate is binding in the region of the molecule around Cys32, then ascorbate should be able to protect APX from being labeled at Cys32. In the presence of 12.5 mM ascorbate, a 100-fold excess over DTNB, the rate of Cys32 modification drops from 0.015 to 0.009 min^{-1}, indicating a modest protective effect. Based on the crystal structure, it is reasonable to expect that ascorbate may not compete well with chemical modification by DTNB. The TNB group is well-ordered in the crystal structure with strong interactions between the TNB carboxyl group and Arg172. Such favorable interactions between the TNB group and protein may account for why such high concentrations of ascorbate are required to give only partial protection.

Activity Using Other Peroxidase Substrates. To further characterize the effects of mutagenesis and thiol modification on APX catalysis, turnover of other common peroxidase substrates was investigated. Figure 9 is the steady-state data of guaiacol turnover. All three proteins exhibited Michaelis−Menten-type kinetics in the presence of guaiacol (Figure 9). The calculated V_{max} for the proteins were 52.9, 103.9, and 80.3 s^{-1} for wild type, Cys32Ser, and APX-TNB, respectively. Thus, not only is guaiacol turnover unaffected by Cys

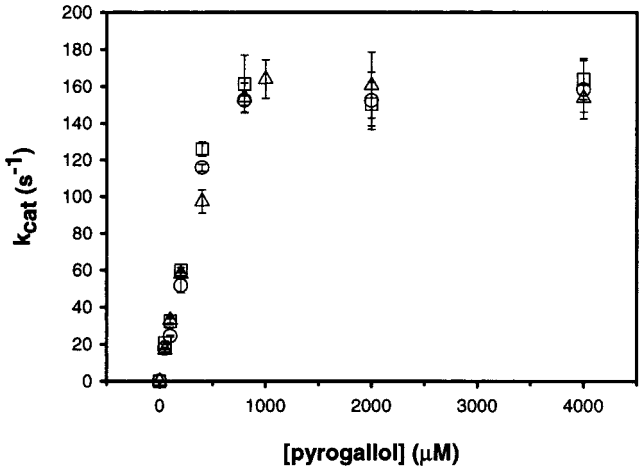

FIGURE 10: Pyrogallol oxidation rates by wild-type APX, Cys32Ser, and APX-TNB. Wild-type APX (○) was assayed at a concentration of 26 nM, Cys32Ser (△) was assayed at a concentration of 27 nM, and APX-TNB (□) was assayed at a concentration of 24.6 nM.

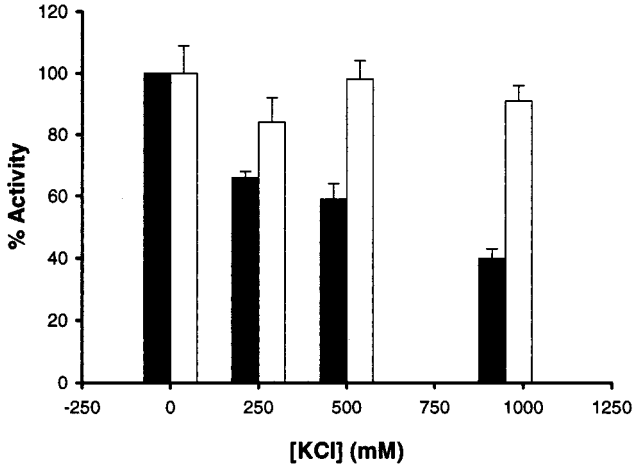

FIGURE 11: Ionic strength dependence on activity. The steady-state ascorbate (black bars) and guaiacol (white bars) oxidation activities were measured in wild-type APX at various KCl concentrations. The activity in 0 mM KCl was arbitrarily set to 100% activity.

mutagenesis or modification, but also the catalytic rate of the mutant increased relative to the wild-type protein. The calculated K_m values for the proteins were 4.2, 6.1, and 9.7 mM for APX, Cys32Ser, and APX-TNB, respectively.

Figure 10 shows the steady-state oxidation of pyrogallol (1,2,3-benzenetriol) by all three proteins. They all exhibited a sharp increase in turnover as the pyrogallol concentration increased and then immediately plateaued at a k_{cat} of ≈160 s^{-1}. These data could not be modeled according to the hyperbolic Michaelis−Menten curves. At the higher pyrogallol concentrations, the reactions proceeded so rapidly, it was difficult to accurately capture the steady-state reactions in the spectrophotometer before they were over (i.e., nonlinear).

Effect of Ionic Strength. Since ascorbate is an anionic substrate and guaiacol and pyrogallol are neutral, it was hypothesized that the region around Cys32 may preferentially bind anions and that enzyme−ascorbate interactions might be governed by electrostatic interactions. To test this possibility, the ionic strength dependence on activity was determined to see if ionic strength inhibits the ascorbate peroxidase activity compared to guaiacol peroxidase activity (Figure 11). The guaiacol peroxidase activity dropped only 9% at the maximum ionic strength tested, 1.0 M., compared to a 60% drop for the ascorbate peroxidase activity. Thus, ascorbate interactions with APX are partly mediated through electrostatic interactions.

If electrostatics are involved in substrate interactions in the Cys32 region, then other anionic peroxidase substrates should exhibit similar decreases in turnover when Cys32 is modified. The steady-state kinetics of the anionic substrate, ferrocyanide, are shown in Figure 12. Unlike ascorbate, the Cys32Ser mutation has little effect on the kinetics of ferrocyanide turnover, but the DTNB modification decreased activity by ≈90% at 300 mM ferrocyanide.

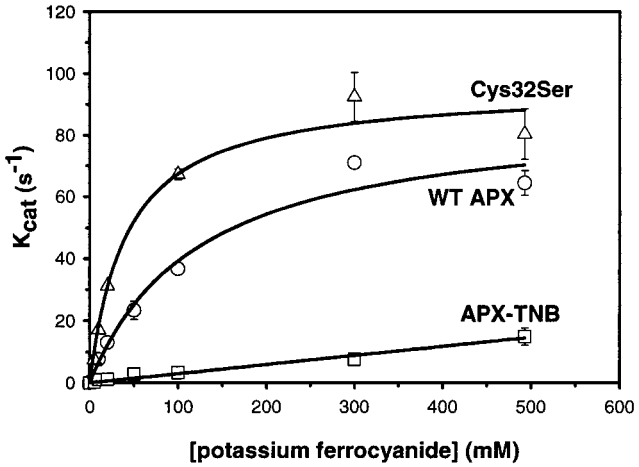

FIGURE 12: Potassium ferrocyanide oxidation rates by wild-type APX, Cys32Ser, and APX-TNB. Wild-type APX (○) was assayed at concentrations of 21.4 and 24 nM, Cys32Ser (△) was assayed at a concentration of 25.8 nM, and APX-TNB (□) was assayed at a concentration of 25.2 nM.

DISCUSSION

Crystallography has proven to be the most powerful tool for mapping out substrate binding sites in enzymes. Unfortunately with peroxidases there are only a limited number of examples. The structure of the CCP−cyt *c* complex is known (*5*) as well as the structure of manganese peroxidase complexed with its substrate, Mn^{2+} (*20*). A third example is the HRP−benzhydroxamic acid (BHA) complex. The HRP−BHA complex reveals an aromatic binding site in a hydrophobic pocket near the δ edge of the heme (*7*). BHA proves to be an optimized substrate for crystallographic studies with peroxidases due to the extensive H-bonding interactions forming a stable enzyme−substrate (ES) complex. We have attempted similar crystallographic experiments with APX using as substrates ascorbate and guaiacol. However, no clear density was observed for either substrate, presumably due to weak interactions between APX and these substrates. The rather large K_m of guaiacol oxidation, 4.2 mM, and the non-Michaelis−Menten behavior of ascorbate oxidation suggest the formation of very "loose" complexes between APX and these substrates. As a result, we have adopted a protein engineering and chemical modification approach coupled with crystallography as tools for mapping out substrate interaction sites in peroxidases.

It was originally hypothesized from the structural homology between the active sites of APX and CCP, especially concerning the homologous tryptophans (191 in CCP and 179 in APX), that similar catalytic mechanisms and electron-

transfer pathways might exist. However, two lines of evidence show this not to be the case. First, the Trp179Phe mutant in APX has no effect on ascorbate peroxidation activity (*21*) while the same mutation, Trp191Phe, in CCP essentially eliminates cytochrome *c* peroxidation activity (*22*). Second, electron paramagnetic resonance (EPR) studies with APX compound I demonstrate the existence of a short-lived porphyrin π-cation radical (*18*) while CCP compound I forms a stable tryptophan radical localized on Trp191 (*23*). Coupled with the crystal structure of the CCP−cyt *c* complex (*5*) and site-specific cross-linking studies (*24*), these results indicate that cyt *c* delivers its electrons to the Trp191 radical but that APX uses some other route.

The obvious choice for ascorbate binding and oxidation is at the exposed δ-meso heme edge (Figure 2) which is supported by recent work on APX (*8*). Addition of ascorbate to APX complexed with cyanide leads to spectral shifts which provides a convenient basis for determining K_D. In addition, since ascorbate leads to spectral changes, it is reasonable to conclude that ascorbate binds near the heme, such as the exposed heme edge. However, the calculated K_D of ascorbate binding is approximately 30-fold smaller than the estimated K_m of ascorbate peroxidation. Therefore, caution must be exercised in associating spectral K_D values with kinetically important ES complexes. In addition to the spectral titration work, Hill et al. (*8*) used NMR methods, molecular modeling, and modification of the exposed δ-meso heme edge with phenylhydrazine, a suicide substrate, to conclude that substrates bind at the δ-meso edge in the vicinity of Ala134.

Our results present a significantly different picture. The steady-state data indicate TNB modification greatly decreases the ability of APX to oxidize ascorbate, yet the enzyme is still fully active when guaiacol is the electron donor. Moreover, only the reductions of compounds I and II are affected by chemical modification and mutagenesis, but not compound I formation. A specific role for Cys32 can be ruled out since the Cys32Ser mutant still exhibits about half the activity of wild-type enzyme in the reduction of both compounds I and II (Table 2). As shown by the crystal structures, this relatively small drop in activity for the Cys32Ser mutant cannot be attributed to significant changes in structure. However, the smaller and more polar Ser side chain will most likely weaken nonbonded interactions with Phe26, Ile27, and Ile36 (Figure 3) which might destabilize the proposed ascrobate binding site. These results suggest that the disulfide-linked TNB adduct selectively inhibits electron transfer from ascorbate by sterically blocking access of ascorbate to an electron-transfer docking site. The ionic strength dependence of ascorbate peroxidation and lack of ionic strength dependence for guaiacol peroxidation further support the view that anionic and neutral substrates interact at different sites. The cryogenic structure of APX-TNB reveals clear density for the disulfide-linked TNB group in a concave region on the surface near the heme propionates and the γ-meso-heme edge (Figures 1 and 2). The TNB is anchored in place by a disulfide bond to Cys32 on one end of the molecule and strong electrostatic interactions with Arg172 on the other end (Figure 2). These same electrostatic interactions may play a role in binding anionic substrates. Therefore, electrostatic masking of Arg172 and steric hindrance have eliminated ascorbate and decreased ferrocyanide peroxidase activities.

In summary, the present work has led to the following simple and testable working hypothesis. Anionic substrates, including ascorbate, bind to APX near the heme edge containing the propionates by possibly interacting with Arg172. Reduction of both compounds I and II occurs at this site. Small uncharged aromatic substrates bind at the exposed heme edge, the favored sites for most peroxidases. Further testing of this hypothesis should open the way for enhancing the specificity of peroxidases using a combination of mutagenesis, chemical modification, and molecular modeling.

ACKNOWLEDGMENT

We thank Dr. David J. Schuller, Dr. Huiying Li, and Dr. M. Sundaramoorthy for expert crystallographic advice.

REFERENCES

1. Dunford, H. B. (1982) *Adv. Inorg. Biochem. 4*, 41−68.
2. Mittler, R., and Zilinskas, B. A. (1991) *Plant Physiol. 97*, 962−968.
3. Poulos, T. L., Freer, S. T., Alden, R. A., Edwards, S. L., Skogland, U., Takio, K., Eriksson, B., Xuong, N., Yonetani, T., and Kraut, J. (1980) *J. Biol. Chem. 255*, 575−580.
4. Poulos, T. L., and Kraut, J. (1980) *J. Biol. Chem. 255*, 10322−10330.
5. Pelletier, H., and Kraut, J. (1992) *Science 258*, 1748−1755.
6. Ator, M. A., David, S. K., and Ortiz de Montellano, P. R. (1987) *J. Biol. Chem. 262*, 14954−14960.
7. Henriksen, A., Schuller, D. J., Meno, K., Welinder, K. G., Smith, A. T., and Gajhede, M. (1998) *Biochemistry 37*, 8054−8060.
8. Hill, A. P., Modi, S., Sutcliffe, M. J., Turner, D. D., Gilfoyle, D. J., Smith, A. T., Tam, B. M., and Lloyd, E. (1997) *Eur. J. Biochem. 248*, 347−354.
9. DePillis, G. D., Sishta, B. P., Mauk, A. G., and Ortiz de Montellano, P. R. (1991) *J. Biochem. 266*, 19334−19341.
10. Chen, G.-X., and Asada, K. (1989) *Plant Cell Physiol. 30*, 987−998.
11. Asada, K., Miyake, C., Sano, S., and Amako, K. (1993) *Plant Peroxidases*: *Biochemistry and Physiology* (Welinder, K. G., Ramusen, S. K., Penel, H., and Greppin, H., Eds.) pp 243−250, University of Geneva, Geneva, Switzerland.
12. Ho, S. N., Hunt, H. D., Horton, R. M., Pullen, J. K., and Pease, L. R. (1989) *Gene 77*, 51−59.
13. Sanger, F., Nicklen, S., and Coulson, A. R. (1977) *Proc. Natl. Acad. Sci. U.S.A. 74*, 5463−5467.
14. Patterson, W. R., and Poulos, T. L. (1994) *J. Biol. Chem 269*, 17020−17024.
15. Collaborative Computing Project, N. (1994) *Acta Crystallogr. A 50*, 760−763.
16. Brunger, A. T. (1993) Yale University Press.
17. Jones, T. A. (1982) *Computational Crystallography*, Oxford University Press, Oxford, U.K.
18. Patterson, W. R., Poulos, T. L., and Goodin, D. B. (1995) *Biochemistry 34*, 4342−4345.
19. Mandelman, D., Schwarz, F. P., Li, H., and Poulos, T. L. (1998) *Protein Sci. 7*, 2089−2098.
20. Sundaramoorthy, M., Kishi, K., Gold, M. H., and Poulos, T. L. (1994) *J. Biol. Chem. 269*, 32759−32767.
21. Pappa, H., Patterson, W. R., and Poulos, T. L. (1996) *JBIC 1*, 61−66.
22. Mauro, J. M., Fishel, L. A., Hazzard, J. T., Meyer, T. E., Tollin, G., Cusanovich, M. A., and Kraut, J. (1988) *Biochemistry 27*, 6243−6256.
23. Sivaraja, M., Goodin, D. B., Smith, M., and Hoffman, B. M. (1989) *Science 245*, 738−740.
24. Pappa, H., Tajbaksh, S., Saunders, A. J., Pielak, G. J., and Poulos, T. L. (1996) *Biochemistry 35*, 4837−4845.
25. Kraulis, P. (1991) *J. Appl. Crystallogr. 24*, 946−950.
26. Evans, S. V. (1993) *J. Mol. Graphics 11*, 134−138.

BI981958Y